

Published in final edited form as:

Int J Med Robot. 2009 June ; 5(2): 223–231. doi:10.1002/rcs.254.

HyBAR: hybrid bone-attached robot for joint arthroplasty

S. Song^{*}, A. Mor, and B. Jaramaz

Institute for Computer Assisted Orthopaedic Surgery, Western Pennsylvania Hospital, Pittsburgh, PA, USA

Abstract

Background—A number of small bone-attached surgical robots have been introduced to overcome some disadvantages of large stand-alone surgical robots. In orthopaedics, increasing demand on minimally invasive joint replacement surgery has also been encouraging small surgical robot developments. Among various technical aspects of such an approach, optimal miniaturization that maintains structural strength for high speed bone removal was investigated.

Methods—By observing advantages and disadvantages from serial and parallel robot structures, a new hybrid kinematic configuration was designed for a bone-attached robot to perform precision bone removal for cutting the femoral implant cavity during patellofemoral joint arthroplasty surgery. A series of experimental tests were conducted in order to evaluate the performance of the new robot, especially with respect to accuracy of bone preparation.

Results—A miniaturized and rigidly-structured robot prototype was developed for minimally invasive bone-attached robotic surgery. A new minimally invasive modular clamping system was also introduced to enhance the robotic procedure. Foam and pig bone experimental results demonstrated a successful implementation of the new robot that eliminated a number of major design problems of a previous prototype.

Conclusions—For small bone-attached surgical robots that utilize high speed orthopaedic tools, structural rigidity and clamping mechanism are major design issues. The new kinematic configuration using hinged prismatic joints enabled an effective miniaturization with good structural rigidity. Although minor problems still exist at the prototype stage, the new development would be a significant step towards the practical use of such a robot.

Keywords

bone attached robot; hybrid kinematic configuration; miniaturization; minimally invasive clamping

Introduction

Early generation active surgical robots in orthopaedics were typically large and heavy stand-alone devices such as ROBODOC (1) and CASPAR (2). The attempt to bring the advantages of robot technology into surgery often resulted in simply bringing a modified industrial robot into the operating room. Recently, small bone-mounted robots have been introduced in order to overcome various disadvantages of large and heavy stand-alone surgical robots. It appears that a specifically designed small robot that is attached onto its target is a successful solution for target immobilization, which is a major issue in robotic

surgery (3–5). One such robot is a mini bone-attached robotic system (MBARS) developed for patellofemoral joint arthroplasty (6). This hexapod robot demonstrated satisfactory performance for the given task in the experimental set-up. However, it also had some disadvantages, especially for surgical use. Based on the observed problems and limitations of that system, finding an optimal kinematic configuration was the major focus of this research, since the majority of problems and limitations in the original system were related to its mechanical design. The purpose of this study was to redesign the platform so that the key advantages of the parallel robotic structure were maintained, while making the surgical site more accessible for intervention and observation. We approached this problem by looking at kinematic mechanisms that maintained the structural rigidity of a typical parallel platform while reducing the number of degrees of freedom to the bare minimum. Our approach also attempted to move the majority of the mechanism out from around the cutting tool, thereby increasing surgeon visualization and access to the operative site.

Materials and Methods

Background

At the early stage of the research, problems and limitations of the MBARS design were identified. The design of the kinematic configuration of the robot was identified as the main challenge to overcome in order to reach the goals of this research. Another major issue that significantly affects the robot performance was found in the manufacture and assembly of the prototype.

Limitations of MBARS design—The original MBARS was developed as a surgical implementation of a standard Stewart platform parallel robot equipped with a cutting device (TPS, Stryker Instruments, Kalamazoo, MI). A number of benefits of the typical parallel robot structure met the requirements of robotic patellofemoral joint arthroplasty surgery. However, while the preliminary design was used to successfully prove the concept, it suffered from several problems that prevented its consideration for clinical use:

- *Sterilization*: the first and most important problem was that the robot was not sterilizable and would be very difficult to protect with a sterile bag.
- *Accuracy*: the original design suffered from low accuracy because of inherent structural compliance and because of the use of insufficiently accurate components, such as ball joints and ball screws.
- *Workspace*: the high-speed cutting tool is surrounded by the parallel robot structure, which can be an advantage for a surgical robot in terms of safety aspects. However, in order to provide the required manipulation of the cutting tool, the parallel robot requires a relatively large structure (compared to a typical serial robot that has similar workspace), resulting in a larger and heavier robot, negating the approach of a mini bone-attached surgical robot.
- *Accessibility*: the surgical target and cutting tool are located at the centre of the robot structure, so they are almost unreachable from outside the robot. It could be advantageous that the surgical area is isolated from external interruption if the surgeon's manual access is not required during the autonomous procedure. In practice, however, the surgeon needs to be able to pause the robot and access the target manually at any time during the surgery. If access is significantly limited by the robot structure itself, it can be a major disadvantage of robotic surgery.
- *Mounting structure*: the bone-mounting mechanism that connects the robot manipulator to the target bone is important, since it determines the rigidity and therefore the stability of the robot system. Although it is difficult to quantify the

level of immobilization, secure clamping on the target bone must be achieved in order to deliver precise robotic manipulation. A modular mounting structure that attaches to the target, securely providing a rigid base frame for the robot, is preferred.

- *Complexity*: based on the cutting geometry, a minimum of three degree-of-freedom (DoF) manipulation is required, which can be achieved by a combination of prismatic and rotational joints. However, the typical parallel robot consists of six closed joints delivering six-DoF manipulation. The extra joints can provide higher speed and strengthen structural stability, nevertheless, the specific surgical task requires low-speed manipulation and the robot's structural stability can be obtained by adding passive structure rather than additional active joints.

To remove or minimize the disadvantages of the typical parallel robot structure, the optimal kinematic configuration that meets the requirements of the proposed robotic surgery was investigated.

Kinematic considerations—With respect to kinematic configuration, manipulators can be divided into serial or parallel. In general, serial manipulators have a larger workspace with respect to their own volume and a grounded base space. However, because of its low structural stiffness and accumulated joint errors, large motors and/or high gear ratio transmissions are often used with a strong link body, resulting in large and heavy robots overall. Parallel manipulators, on the other hand, have increasing structural stiffness as more links are connected to the end effector. This multiple linkage structure also averages linkage errors, so that higher accuracy can be achieved. However, typical parallel manipulators have limited workspace, due to mechanical joint limits and collision of links. Based on the features of serial and parallel manipulators, it is noted that early-generation surgical robots have typical serial manipulator problems and yet their designated task area is very isolated despite having a large available workspace. In other words, a serial configuration may not be the optimal choice for the surgical tasks. On the other hand, the hexapod type of bone-attached robot benefits from the advantages of a parallel manipulator in terms of weight and structural rigidity. However, it also has the disadvantages of parallel structures, such as limited workspace, relatively large grounded base and the complexity of the six-DoF robot. From such observations, it was concluded that a serial structure is less suitable than parallel structures for surgical robots that aim to be light enough to attach onto bone and maintain rigidity against significant external forces (e.g. reaction forces from high-speed bone cutting). Besides, the known disadvantages of a parallel structure are mainly based upon a typical hexapod robot. Hence, we investigated new parallel structures that have the benefit of closed-chain linkage and can avoid the disadvantages of a typical hexapod.

Prototype development

In patellofemoral resurfacing, bone shaping with a high-speed burr cutter involves mainly planar motion, with a relatively shallow depth of cutting in the third direction. Based on that, two simple kinematic concept models were designed (Figure 1a, b). Figure 1a is a three-DoF parallel manipulator that consists of three hinged (free rotation) translational joints covering a Cartesian workspace, and a hybrid model (Figure 1b) that has two hinged translational joints creating X - Y planar movement, which is serially linked to a vertical Z axis. Since structural rigidity was mainly required in the X - Y plane, and to simplify inverse kinematic computation (motion in X - Y and Z can be decoupled and controlled separately for faster response), the hybrid model (Figure 1b) was selected as the new kinematic configuration.

For the translational joints (two hinged arm joints for X - Y planar motion and a vertical joint), an anti-backlash leadscrew-nut mechanism was selected. An assembly of 3/16 inch

nominal diameter with 1/10 inch pitch leadscrew and spring loaded anti-backlash nut (Kirk Motion 3000 series leadscrew and NTGY nut) were selected as the smallest off-the-shelf parts available. The nut is connected to a linear slide rail (Del-Tron DP series Precision Linear Guides) so that the leadscrew rotation is transmitted to prismatic motion. Another linear slide carriage is attached to the nut where the rail is a part of the framework in order to support the overall mechanism. At the maximum extension of the prismatic joint, the out-of-plane position error is greatest. This is the largest error component present in the overall robot structure. In order to maintain the rigid triangular structure at all times, the leadscrew mechanism is non-backdrivable. In other words, the structure can be considered as a non-moving rigid structure against any external force, such as the reaction of the robot's manipulation and unexpected accidental forces. To achieve this, the lowest possible pitch (2.54 mm) was selected. A belt pulley transmission mechanism was selected to build all three axes, since it is simple and backlash-free. The leadscrew is connected to a motor that is located in parallel by a timing belt and pulley, which also allows the use of different gear ratios. A 1.8 mNm DC servo motor with 161 : 1 zero backlash spur gearhead was selected for the powertrain. A 12 counts/turn encoder that provides 48 counts/revolution quadrant signal was assembled with the powertrain (Faulhaber DC-Micromotor Series 1224, Series 12/5 gearhead and HE Series encoder). The belt transmission ratio is 10 : 12 for the X - Y planar arms and 10 : 14 for the vertical Z axis. Through motor, gear, belt and leadscrew transmission, the overall resolution of the robot is 0.282 μm in the X - Y plane and 0.235 for the Z axis. An end effector holder was designed to connect the tip of the two horizontal arms, so that each arm is hinged together at the same axis where the surgical tool is fastened. The holder is designed to fasten a mid-sized drill attachment shell (Stryker TPS) instead of a drill body into the hinged end effector axis. Figure 2a shows a CAD model of the overall robotic system.

A new bone-mounting structure (shown in Figure 2b) was designed to fit into the surgical opening with little or no extension to the typical incision and to provide a secure base for the robot. The structure has three bone screw or pin insertion points, in order to fasten the mounting structure to the target bone as a solid structure. In order to allow various robot mount angles, a lockable ball joint was used to attach the robot to the bone mount. This allows an initial manual positioning of the robot. Unlike the original MBARS, the detachable modular bone-mounting approach enables a greater possibility of implementing robotic surgery on various surgical applications with only minor changes. For instance, the robot can be used for cranial surgery by replacing the bone-mounting structure with a customized mounting structure. In general, frameworks of prototype robots are usually made of aluminium, due to low cost and easy manufacture. However, size and weight of this prototype are key properties for the bone-attached approach, so medical-grade stainless steel was chosen as the manufacturing material. Therefore, the feasibility of this bone-mounted robot prototype can be assessed in a more realistic manner. The choice of material also affects the compactness of robot design (e.g. the framework can be thinner with stronger material). Without the surgical drill and the three bone screws, the robot prototype (including motors) weighs approximately 1 kg. With a TPS drill installed, the total weight is still less than 1.5 kg. Figure 2c shows the manufactured robot prototype. Considering that lighter orthopaedic drills are available, the total weight of the prototype indicates that the bone-mounted robotic surgery approach is adequate as long as the bone cutting does not create a significant reaction force. In other words, the cutting feed rate must be controlled to prevent creating excessive reaction force.

An industrial standard high-bandwidth motion controller with embedded amplifier was used for motion control, and is powered by a 24 V bipolar power supply. A Pentium III host PC is linked to the controller via Ethernet connection. The capability of using an existing Ethernet network, instead of direct connection, such as via serial port or USB, allows the host PC and

technical operator to be located outside the operating room. Moreover, in principle, a single host PC can be used to control multiple simultaneous operations with a centralized process and data.

Path planning and surgical planning

The goal of path planning for a robotic system such as this is to end up with a cavity in the bone properly shaped for the implant, so that the implant will be placed in the planned position. Due to the fact that the implants have a fixed shape, this path planning can be done offline and then placed, along with the implant CAD model, on the preoperatively constructed CT during the surgical planning step (Figure 3a). The bottom surface of the implant is the shape used for path planning, as that is the surface that must match up to the cavity in the bone.

The main constraints on the path-planning step are the non-zero radius of the spherical cutting burr and accounting for the scallop height (7) between neighbouring passes of the cutting burr. Because the cutting burr has a non-zero radius and the commanded positions for the robot correspond to the centre of the cutting burr, we cannot just find points on the surface of the implant as robot positions. The points for the robot to visit must be set back from the surface one cutting burr radius to ensure that the burr is tangent to the surface at that point. But scallops between cutting passes must be taken into account. If the robot made two parallel passes a certain distance apart, a small peak would be formed halfway between the passes. Figure 3c shows a cross-section of the scallop formed between parallel cutting passes, where the light grey area is the volume to be removed by the dark grey cutting burr, and the scallops are shown in white. If the cutting burr was always one radius above the surface of the implant, then the scallops would protrude into the desired location of the implant, and the implant would not end up in the desired location. Therefore, the scallop height for a given distance between passes is calculated, and the height of the centre of the cutting burr over the implant surface is reduced by this scallop height. This will lower the scallops down and bring the peaks of the scallops down to the implant surface.

The first step in the path-planning process is picking points along the centre line of the implant that will define the direction of the back-and-forth passes. Then the best-fit plane to the bottom of the implant is calculated, which defines the principal direction that the implant would be placed into the bone cavity. After this, a plane is rotated around the centre of the implant and the furthest intersections of this plane and the implant surface define the path around the outside of the cavity that will generate a smooth outer cut surface. These points, however, lie on the surface, so they are projected back towards the centre of the implant one burr radius. They are then moved in the principal direction described above until they are the correct height, the burr radius less the scallop height, above the surface. After the outline path is determined, then a grid of points is defined below the surface and projected along the principal direction to find the intersections with the surface that define the back-and-forth path. These points are also moved so that they are the correct height above the surface. The outline path is then connected to the inner back-and-forth path to define the cutting path that will generate the bottom surface of the cavity in the bone. This path is repeated a number of times above the bottom surface, so that the robot does not attempt to take too large a cut. The path is then saved. Figure 3b shows an example of a planned cutting path.

After the implant location is planned and the robot position on the bone is determined, the saved path is transformed into the robot's reference frame for the actual cutting. Preoperative surgical planning is based on our preoperative planners for hip and knee surgery. In the planner, a surface model of the bone, typically built from a preoperative CT scan, is rendered both in surface form and in three cross-sectional views. The surface model of the implant is also rendered in those views, and the user or surgeon can change the

location and orientation of the implant relative to the bone. Once the surgeon is satisfied with the position of the implant relative to the bone, a surgical plan is saved and used during the intraoperative registration and cutting of the femur.

Prototype evaluation

To determine the speed and accuracy of the robot prototype during cutting, we performed bone-cutting experiments on foam femur phantoms and pig femurs. Figure 4a, b show the experimental set-up. These tests provided us with experience in setting up the robot, planning the location of the implant on the bone, determining the relative position of the robot and the bone, and final cutting speed and accuracy. The foam phantoms were utilized as a simple first test for cutting performance, where each bone had the same shape and the material was easy to cut. The pig bones were a more direct analogue to cadaver testing, where bone hardness was a close approximation to human bone hardness and individual planning for each femur was required.

The process utilized for the test on the foam bones and the pig bones was identical. The first step in this testing was the acquisition of a CT scan of the bone and the segmentation of the femur anatomy from that scan. Utilizing a customized version of our preoperative surgical planner, a model of a femoral implant was placed in a suitable position on the femur. The goal in the placement of the implant was to have the main axis of the implant aligned with the patellofemoral joint, and the outer edges of the implant either congruent with, or slightly inset from, the surface of the bone. After the surgical plan was completed, the robot's mounting clamp was attached to the bone and the robot was mounted on the clamp so that the cutting tool was directly above the expected cutting area. At this point, the robot was then registered to the bone using the Certus optical tracking system (Northern Digital Inc., Ontario, Canada) The first step in the registration is to determine a coarse registration between the robot and the bone by collecting the location of three known points on the robot and a number of points on the femur. The computer system can then determine the relative position of the robot and the bone. However, due to the small baseline of available points on the robot's base, the accuracy of this registration was not sufficient. Therefore, the robot was then commanded to a set of three points surrounding the cavity to be milled. For each of these three points, we collected the position of the tip of the cutting tool. This gave us a much better baseline for registration and the points used for registration were very close to the operative site. Quantitatively, tool tip positioning errors from the coarse method were easily in the order of 2.0 mm, whereas errors from the final registration were in the order of 0.2 mm.

After registration was performed, the cutting path corresponding to the planned implant location was transformed into the robot's workspace, the cutting burr was installed into the cutting tool and the bone was cut. The location of the cutting burr was recorded with the tracking system during the cutting process (Figure 5). After the cut was completed, a cloud of points from the milled cavity was collected to help measure the shape of the cut, and a postoperative CT of the bone was also acquired and segmented. Due to the small number of tests run (four foam femur phantoms and three pig femurs), descriptive statistics were compiled for each of the bones. The first part of the analysis looked at the overall shape of the milled cavity and the second part looked at the location of the cavity relative to its planned location.

Results

Two sets of data were used for the first part of the analysis: the first was the surface model of the cavity from the postoperative CT; the second was the cloud of points collected with the optical tracking system. For the first set of data, shown in Table 1, the best fit of the

surface geometry of the implant to the cavity in the postoperative bone model was computed, and then distance metrics between the implant surface and the cavity were calculated, using the Mesh (8) program (Figure 6). For the second set of data, shown in Table 2, we fitted the surface model of the implant to the cloud of points from the cavity, and report the distance metrics between the cloud of points and the final position of the implant model. Mean values in this table are zero-based on the iterative closest point method used to fit the two models and calculate the errors.

In Table 3, the second part of the analysis looked at the average error between the planned location of the implant and the location of the milled cavity, determined from the postoperative CT scan. One major issue became evident during the pig bone cutting tests but not during the foam bone cutting. While the cutting burr was able to cleanly cut the pig bone, every bone implant was displaced in the positive Z direction, indicating that the bone-cutting reaction force was deforming the robot structure a measurable amount. Burr locations during cutting shown in Figure 5 were typical, with the burr locations while cutting bone displaced up and away from the surface being cut, while the foam bone models demonstrated more of a rotational displacement.

Each pig bone test, which included two passes of the burr to reach final depth, took 410 s on average from the start of robot motion to the end of cutting, with individual passes 1.5 mm apart. The time for cutting was basically deterministic, because each cutting path covered the same path in space, varying only by the small differences in implant position relative to the robot's reference frame. Each foam bone test, where three passes were used due to a thicker implant model, took an average of 602 s. Implant fitting precision, as measured by the shape of the cavity, not its position, was better than 2.0 mm under all tests, and the maximum displacement from the planned position of the implant was 2.46 mm (foam No. 1 from Table 3), which is a combination of errors in registration accuracy and cutting precision. In the foam bone, qualitative fit between the implant and cavity was quite good, with a snug friction fit. Figure 7 shows examples of the experimental results.

Discussion

We developed a manipulator mechanism optimized for enhanced structural rigidity, weight reduction and greater workspace usage under the given surgical task conditions of patellofemoral joint arthroplasty. Based on our experiments, we were able to consistently show overall precision in cutting pig bones on the order of 0.2–0.37 mm, depending on the measurements utilized. One drawback, however, was the relatively large average displacement of the implant, which could be attributed to cutting reaction forces and insufficient rigidity in the structure of the robot.

Cutting with this robot should provide a cavity that would suitably constrain an implant for a precise fit, based on the fit between the implant and bone shown in Figure 7b. Although the overall accuracy is probably sufficient for practical use, the vertical structure of the robot seems relatively weak against bending when cutting bone. Also, the burr used was fairly dull, probably increasing the cutting reaction force. From a practical usage standpoint, for sterilization purposes the robot can be simply bagged. However, further mechanical design optimization, while maintaining the benefits of the new kinematic design, may be required to facilitate the sterilization. As one possible design solution, an embedded telescope-like robot design is proposed for future development. Mechanical parts such as the powertrain and transmission can be placed inside a sealed extendable cylindrical robot arm, so that the robot can deliver the same manipulation. Also, the cylindrical arm structure should provide greater rigidity against bending and buckling.

Patellofemoral resurfacing is a relatively low-volume procedure. It is intended for patients who are younger and more active than the traditional arthritic population, where it makes sense to limit the surgical reconstruction to the area involved in the degeneration (9). While the target application of HyBAR was limited to patellofemoral resurfacing, it would be relatively easy to extend its application to several other procedures. From a practical standpoint, it would be beneficial to design the robot as a limited multi-purpose robot handling, e.g. several bone-shaping procedures that require a similar workspace, such as unicondylar knee replacement or, potentially, a more conservative bone-sparing total knee replacement. As no procedure other than patellofemoral resurfacing can be planned solely on the basis of local information collected within the workspace of the robot, it makes more sense to design a robot that works within the standard framework of surgical navigation and includes external large-volume position tracking. This does not take away any of the benefits of the robotic procedure performed with a small, bone-mounted robot as originally outlined, but expands its clinical potential. In terms of control, preplanned feed-rate control and real-time implicit current control can be implemented. Both control algorithms reduce the reaction force from bone cutting in order to prevent large bone chipping and failure of the surgical tool, which can occur by excessive cutting. Tool feed rate can be planned based on cutting volume, since the amount of cutting in any given move is known. The system current value can also be monitored in real time to adjust the speed of cutting. These enhancements should facilitate improved outcomes.

We have shown that, through careful consideration of the design constraints, it is possible to build a lightweight bone-attached robot to control the motion of a surgical cutting tool. Precision was shown to be, on average, <0.37 mm, and the worst overall positioning of the implant was measured at 2.46 mm. These errors will improve with further development and refinement of the basic HyBAR concept.

Acknowledgments

This work was supported by the National Institutes of Health under NIH R01 Grant No. AR052700.

References

1. Cohan S. ROBODOC achieves pinless registration. *Indust Robot*. 2001; 28(5):381–386.
2. Peterman, J.; Kober, R.; Heinze, P., et al. Implementation of the CASPAR system in the reconstruction of the ACL. Annual Meeting of Computer Assisted Orthopaedic Surgery (CAOS)/ USA; Pittsburgh, PA, USA. 15–17 June 2000; p. 86-87.
3. Barzilay Y, Liebergall M, Fridlander A, et al. Miniature robotic guidance for spine surgery – introduction of a novel system and analysis of challenges encountered during the clinical development phase at two spine centres. *Int J Med Robot*. 2006; 2 (2):146–153. [PubMed: 17520625]
4. Hanndorff, M.; de la Fuente, M.; Wirtz, DC., et al. Development of a new miniaturized robotic device for the removal of femoral bone cement. 5th Annual Meeting of Computer Assisted Orthopaedic Surgery (CAOS) – International Proceedings; Helsinki, Finland. 19–22 June 2005; p. 138-139.
5. Plaskos C, Cinquin P, Lavalley S, et al. Praxiteles: a miniature bone-mounted robot for minimal access total knee arthroplasty. *Int J Med Robot*. 2005; 1(4):67–79. [PubMed: 17518407]
6. Wolf A, Jaramaz B, Lisien B, et al. MBARS: mini bone-attached robotic system for joint arthroplasty. *Int J Med Robot*. 2005; 1(2):101–121. [PubMed: 17518383]
7. Abraham N, Wolf A, Choset H. A potential function approach to surface coverage for a surgical robot. *Comput Aided Surg*. 2006; 11 (1):1–9. [PubMed: 16531337]
8. Aspert N, Santa-Cruz D, Ebrahimi T. MESH: Measuring error between surfaces using the Hausdorff distance. *Proceedings of the IEEE International Conference on Multimedia and Expo (ICME)*. 2002; 1:705–708.

9. Cannon A, Stolley M, Wolf B, et al. Patellofemoral resurfacing arthroplasty: literature review and description of a novel technique. *Iowa Orthop J.* 2008; 28:42–48. [PubMed: 19223947]

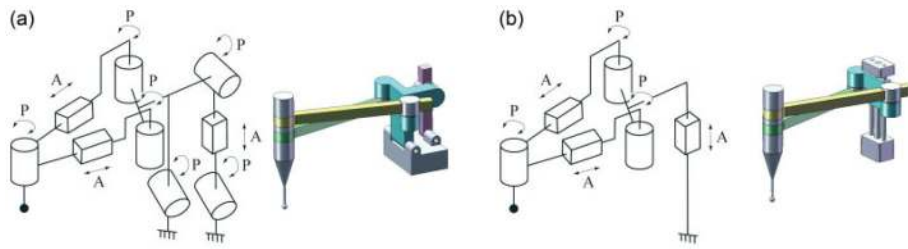


Figure 1. Schematic and CAD model of (a) three DoF parallel kinematic configuration and (b) two DoF parallel and one DoF serial hybrid kinematic configuration. A, active joint; P, hinged passive joint

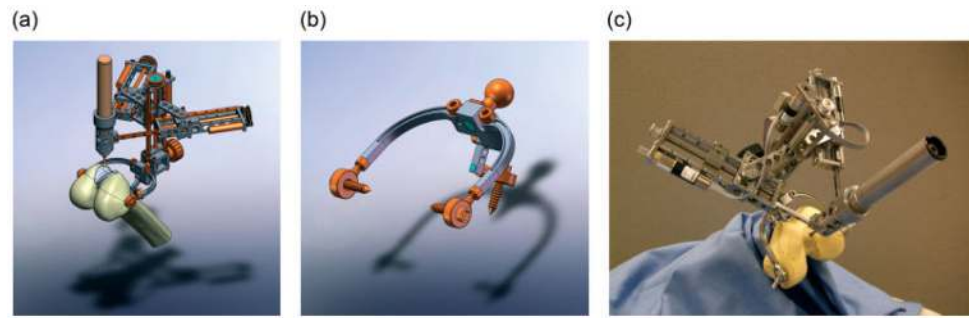


Figure 2. CAD model of (a) overall robotic system mounted on femur with femoral implant, (b) bone-mounting structure and (c) manufactured robotic system

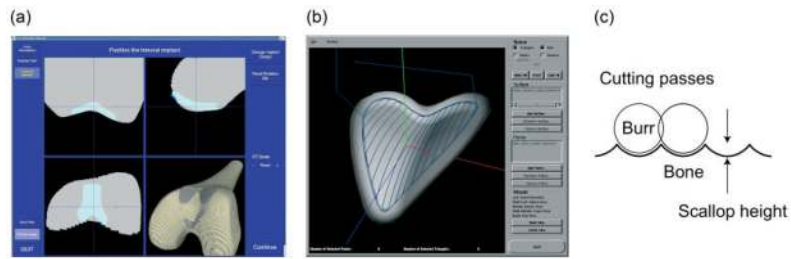


Figure 3.

(a) Screen shot of the preoperative planner, with surface rendering in the lower right and three orthogonal cross-sectional views. (b) An example of the planned cutting path. (c) Diagram of scallop between successive cutting passes

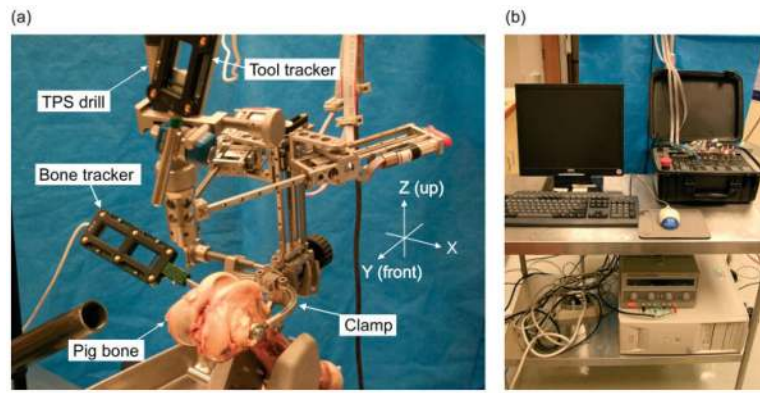


Figure 4. Experimental set-up shows: (a) the robot and mounting structure placed on a pig femur with optical trackers for the robot's base frame and tool tip; (b) host PC connected with the controller via Ethernet

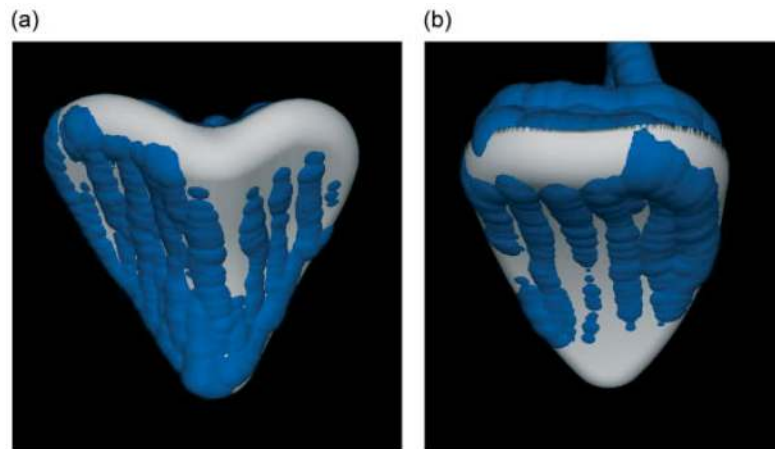


Figure 5. The location of the cutting burr collected with the Certus during cutting, shown with the planned location of the implant for (a) foam No. 2 and (b) pig No. 1

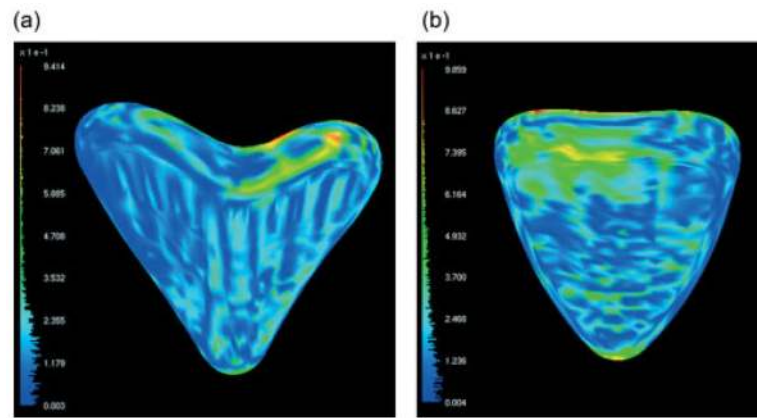


Figure 6. Output from Mesh, showing the distance between the implant and the cavity in the bone for (a) foam No. 2 and (b) pig No. 1

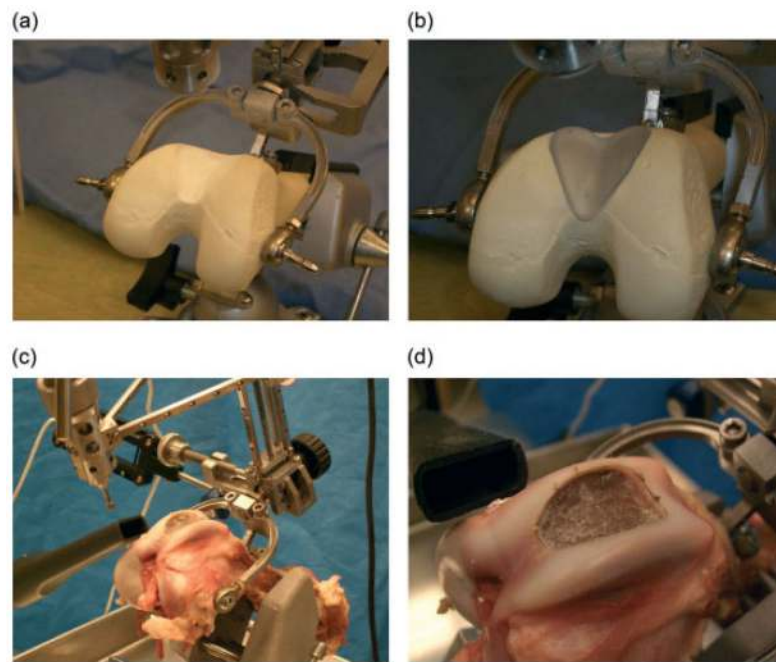


Figure 7. Foam and pig bone experiment results: Foam bone (a) post-cut cavity, (b) a rapid prototype sample implant fitted in the cavity and pig bone (c) post-cut cavity and (d) implant cavity views (an implant CAD model was created for pig's femoral joint replacement)

Errors (mm) between the geometry of the implant and the milled cavity acquired from the postoperative CT scan. Values calculated by Mesh (8)

Table 1

	Foam No. 1	Foam No. 2	Foam No. 3	Foam No. 4	Pig No. 1	Pig No. 2	Pig No. 3
SD	0.12	0.12	0.13	0.10	0.13	0.13	0.15
Mean	0.17	0.16	0.18	0.16	0.20	0.18	0.19
Maximum	1.27	0.94	1.12	1.36	0.99	1.04	1.20

Table 2

Errors (mm) between the cloud of points collected after cutting and the geometry of the implant. Values calculated by point to surface registration program

	Foam No. 1	Foam No. 2	Foam No. 3 ¹	Foam No. 4	Pig No. 1	Pig No. 2	Pig No. 3
SD	0.23	0.21	N/A	0.23	0.24	0.24	0.37
Maximum	1.36	0.82	N/A	1.88	1.20	0.82	1.45

¹The cloud of points was not collected for foam No. 3.

N/A, not applicable.

Average and maximum point-to-point displacement (mm) between the implant model that best fitted the cavity after cutting and the planned position of the implant

Table 3

	Foam No. 1	Foam No. 2	Foam No. 3 ¹	Foam No. 4	Pig No. 1	Pig No. 2	Pig No. 3
Average displacement (X, Y, Z)	-0.258	-1.018	-0.167	0.293	-0.275	-0.185	0.146
	1.119	-0.015	0.234	0.205	0.247	0.019	0.097
	-1.969	-0.628	0.050	-0.213	0.740	0.197	1.094
Maximum displacement (X, Y, Z)	-0.550	-0.593	-0.028	0.944	-0.347	-0.197	0.048
	1.685	-0.031	0.842	0.314	0.151	0.017	0.099
	-1.712	-1.620	0.593	-0.675	1.241	0.294	1.599

¹This displacement was calculated by matching the preoperative and postoperative CT models, and then determining the relative positioning of the implants from those two scans.